




Extreme sensitivity of the vortex state in *a*-MoGe films to radio-frequency electromagnetic perturbation

Surajit Dutta, Indranil Roy , Soumyajit Mandal, John Jesudasan, Vivas Bagwe, and Pratap Raychaudhuri ^{*}
Tata Institute of Fundamental Research, Homi Bhabha Road, Mumbai 400005, India

 (Received 23 September 2019; revised manuscript received 13 November 2019; published 30 December 2019)

Recently, detailed real-space imaging using scanning tunneling spectroscopy of the vortex lattice in a weakly pinned *a*-MoGe thin film revealed that the vortex lattice melts in two steps with temperature or magnetic field, going first from a vortex solid to a hexatic vortex fluid and then from a hexatic vortex fluid to an isotropic vortex liquid. In this paper, we show that the resistance in the hexatic vortex fluid state is extremely sensitive to radio-frequency electromagnetic perturbation. In the presence of very low-amplitude excitation above few kilohertz, the resistance increases by several orders of magnitude. On the other hand, when the superconductor is well shielded from external electromagnetic radiation, the dissipation in the sample is very small and the resistance is below our detection limit.

DOI: [10.1103/PhysRevB.100.214518](https://doi.org/10.1103/PhysRevB.100.214518)

I. INTRODUCTION

The Abrikosov vortex lattice [1,2] (VL) in a type II superconductor behaves like soft periodic solid. In principle, thermal excitations can melt the crystalline VL into a vortex liquid with increase in temperature or magnetic field [3,4]. Yet observation of vortex liquid states is rare. Many experiments indicate that in bulk three-dimensional superconductors thermal fluctuations alone cannot melt the VL into a liquid state [5,6]. Consequently, the disordered state of the VL resulting from the presence of random pinning is often a vortex glass where thermal fluctuations play an insignificant role. However, in two dimensions (2D) the effect of thermal fluctuations can be greatly amplified. While indications of vortex liquid states have been obtained in several quasi-2D systems such as weakly pinned superconducting films [7,8] and organic superconductors [9], compelling evidence of VL melting has been obtained only in layered high- T_c cuprates [10–12] at elevated temperatures.

Recently, evidence of vortex liquid states existing down to very low temperatures has been obtained from detailed scanning tunneling spectroscopy (STS) imaging of the vortex lattice [13] in very weakly pinned thin films of the amorphous superconductor MoGe (*a*-MoGe). Here the thickness of the film is much smaller than the bending length of the vortices such that the VL is effectively two dimensional. These experiments reveal that the VL in *a*-MoGe melts in two steps with increase in magnetic field or temperature. First, the hexagonal vortex solid (VS) transforms into a hexatic state with short-range positional order but quasi-long-range orientational order at fields of few kOe through proliferation of dislocations. Subsequently at a much higher field, the orientational order is lost through proliferation of disclination giving an isotropic disordered state. Furthermore, in these

experiments the trajectory of each vortex has also been tracked as a function of time obtained by imaging the VL at finite time intervals. It is observed that the vortices have a finite mobility in both the hexatic and isotropic disordered vortex state, consistent with the expectation of a hexatic vortex fluid (HVF) and isotropic vortex liquid (IVL). The transitions from VS to HVF and HVF to IVL were also observed to leave clear imprint on the transport properties. At the first transition a small but finite linear resistance appears, signaling the motion of vortices due to Lorentz force under a subcritical current drive. At the second transition, the linear resistance increases rapidly, reflecting the rapid increase in the mobility of vortices as it enters the IVL state. However, despite this remarkable qualitative agreement between structural and transport measurements, a closer analysis reveals a striking discrepancy. Since STS imaging is a slow measurement, individual vortices can be imaged only when the movement of the vortices is slow, i.e., the diffusivity (D) of the vortices is small. In fact, we estimate the diffusivity, $D < 3.2 \times 10^{-21}$ m²/s (see Appendix A) for fields below 85 kOe. For such a small D the resultant linear resistivity (ρ_{lin}) is expected to be well below measurable limit. Thus, in-principle, no electrical resistance should be observed in the HVF. Recently, it has been reported that the superconducting state in two-dimensional samples of InO_x and NbSe₂ is extremely fragile against external electromagnetic radiation [14]. When the samples were exposed to external radiation the resistance was observed to increase by several orders of magnitude which the authors attributed to overheating of the electrons. This prompted us to investigate the effect of low-frequency electromagnetic radiation in the vortex states of *a*-MoGe.

In this paper, we find that the vortex fluid states in *a*-MoGe are extremely susceptible to low-frequency electromagnetic excitations. When the superconducting sample is well shielded from external electromagnetic radiation using low-pass RC filters, the resistance remains below the sensitivity of our measurement, until the vortices are deep in the IVL

^{*}pratap@tifr.res.in

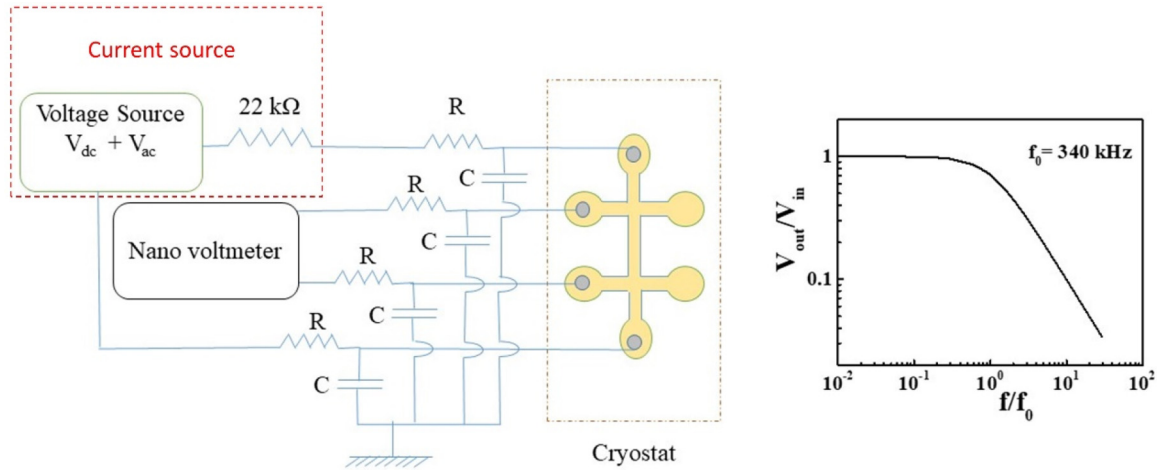


FIG. 1. (Left) Schematic drawing of the four-probe resistance measurements setup. The current is sourced from an ac+dc voltage source in series with a 22-k Ω resistor. For measurements where no ac current is applied a precision current source was used instead. The dc voltage is measured using a nanovoltmeter. RC filters are connected on the electrical feedthrough at room temperature leading to the sample. (Right) Typical frequency response of the RC filter with $f_c = 340$ kHz.

state. However, when a small controlled ac current drive with frequency larger than few kHz is added to the dc measurement current the resistance in the vortex fluid states increases rapidly. We show that this sensitivity is fundamentally linked to the extremely weak pinned nature of the two-dimensional vortex lattice.

II. EXPERIMENTAL METHODS

A. Sample

The sample used in this study is a 20-nm-thick *a*-MoGe thin film grown on surface-oxidized Si substrate with $T_c \sim 7.2$ K, similar to that used in Ref. [13]. The films were grown using pulsed laser deposition using a Mo₇₀Ge₃₀ target prepared by arc melting stoichiometric amounts of Mo and Ge metals. We observed that starting from arc-melted target is essential to obtain *a*-MoGe thin films with low pinning. Samples grown from commercial targets prepared by sintering MoGe powders had similar T_c , but much stronger pinning. Energy-dispersive x-ray compositional analysis of the thin films showed that the latter had a considerable amount of dissolved oxygen which possibly gets incorporated in the sintered targets due to surface oxidation of the powder. The film used for transport measurement was capped with a 2-nm-thick Si layer to prevent surface oxidation and patterned into a Hall bar geometry to improve sensitivity. In contrast, the film used for STS measurements in Appendix A was directly transferred in the scanning tunneling microscope using an ultrahigh-vacuum suitcase without exposure to air.

B. Transport measurements

The schematic of the measurement setup is shown in Fig. 1. The transport measurements were performed down to 300 mK in a ³He cryostat fitted with a superconducting solenoid of 110 kOe. The sample is mounted on a sample rotator where the angle between the normal to the film plane and the magnetic field (θ) can be varied from 0 to 90°.

The default configuration for most measurements was $\theta = 0$. However, the anisotropic response of the vortex state was also investigated by varying θ . To shield the sample from external electromagnetic radiation, room-temperature low-pass RC filters were installed on the electrical feedthrough connected to the sample at the entry point into the metal cryostat. We tried five filters with cutoff frequencies f_c varying between 340 kHz and 7.8 MHz.

Regular dc resistance measurements were performed using the standard four-probe method using a current source and a nanovoltmeter. Current was injected through the outer contact pads using a Keithley 6220 precision current source and the voltage drop across the voltage contacts was measured using a Keithley 2182A nanovoltmeter. To determine the resistance, measurements were done for both positive and negative polarities of current and the corresponding voltages were subtracted from one another to remove any thermopower contribution arising from the sample, contacts, and the leads.

To understand the effect of an ac drive on the dc resistance of the superconductor we also performed measurements by applying a dc current (I^{dc}) superposed with a small ac current (I_f^{ac}). For this the precision current source was replaced with the voltage source of a Stanford Research System SR865A lock-in amplifier in series with a 22-k Ω resistor without altering the rest of the setup. The SR865A voltage source can generate an ac voltage (V^{ac}) of a given frequency, f , superposed on a dc voltage (V^{dc}), such that the current through the sample is $I \cong (V^{dc} + V^{ac})/22$ k Ω . Since the combined resistance of the sample and the connecting wires was ~ 200 Ω , this configuration resulted in a maximum inaccuracy in current of 1% as compared to a true constant-current source. However, in practice the variation in current due to variation in load is much less since the primary load resistance comes from the constantan wires inside the cryostat, which have a very small temperature coefficient of resistance and very small magnetoresistance. Due to the large integration time, only the dc component of the voltage across the voltage contacts is measured with the nanovoltmeter. By measuring standard

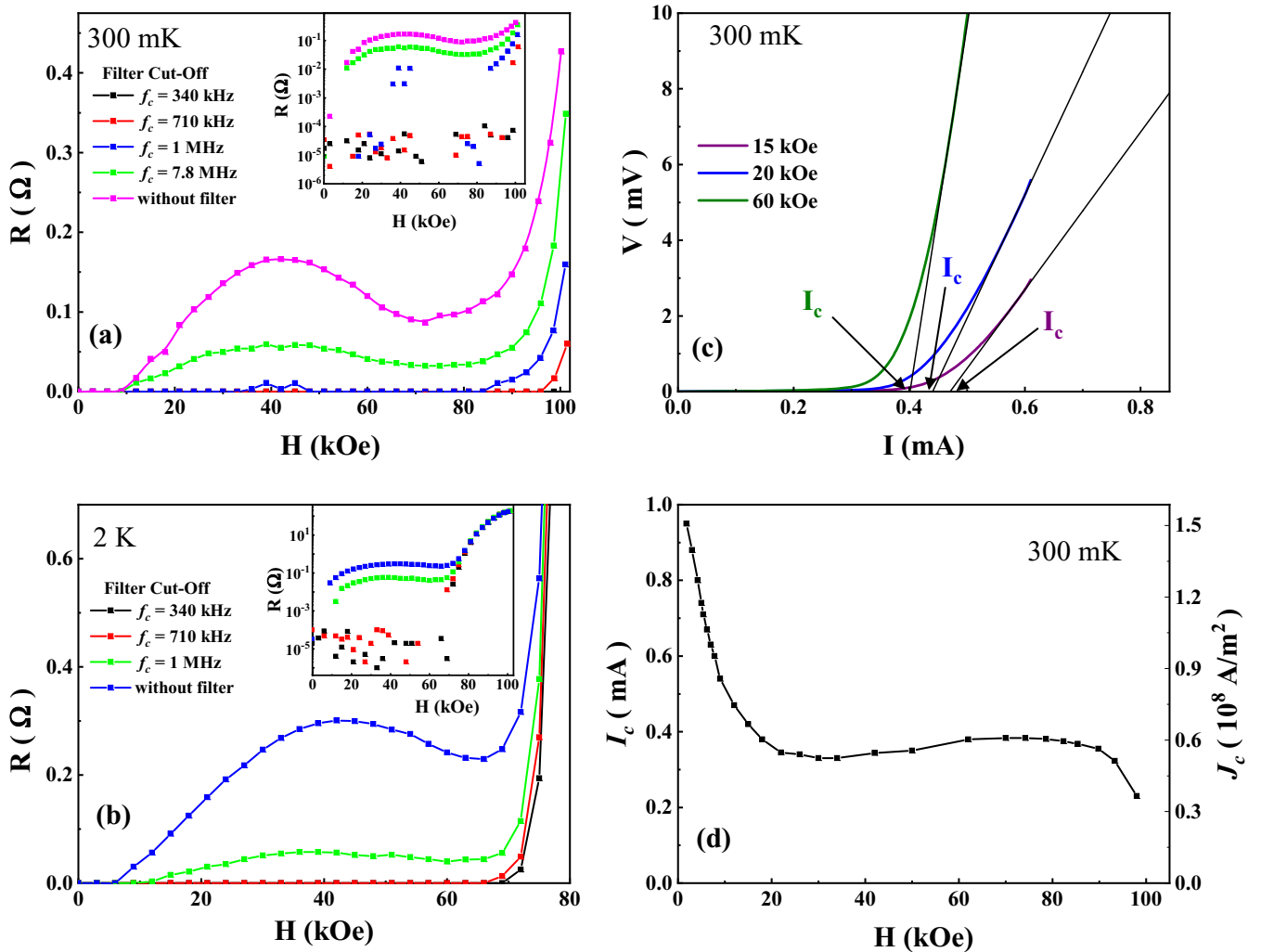


FIG. 2. (a) dc resistance, R , as a function of magnetic field, H , measured at 300 mK with RC filters of different f_c ; (Inset) the same data as in the main plot but plotted in semilog scale. (b) same as (a) but at 2 K. (c) Representative current versus voltage (I - V) characteristics of the film at three different fields at 300 mK from which the flux-flow critical current, I_c , is calculated; I_c is determined by extrapolating back the linear flux-flow regime of the I - V curve. (d) I_c as a function of H at 300 mK; the corresponding critical current density J_c is shown on the right axis.

resistors of different values, we verified that the measured dc voltage in the nanovoltmeter is insensitive to the presence of a small ac voltage for frequencies >500 Hz, both in terms of the mean value and the noise.

C. STS measurements

STS measurements (in Appendix A) were performed in a home-made scanning tunneling microscope [15] (STM) operating down to 350 mK and fitted with a superconducting solenoid of 90 kOe. The VL is imaged by adding a 100 μ V, 2 kHz modulation voltage over the dc bias voltage (V) and recording the tunneling conductance ($G(V) = \frac{dI}{dV}|_V$) over the sample surface using standard lock-in technique. The dc bias voltage is kept close to the superconducting coherence peaks, $V \sim 1.2$ mV. Since the coherence peaks are suppressed inside the vortex cores, each vortex appears as a local minimum in $G(V)$ in the tunneling conductance map. The dc tunneling current during these measurements is fixed at 50 pA. Due to

stringent requirements of electromagnetic shielding to obtain reliable spectroscopic data at low bias voltages corresponding to typical superconducting energy gaps, the STM has several layers of shielding from external electromagnetic radiation in its default configuration. The entire STM is kept inside a radio-frequency shielded metal cage and all electrical inputs are fitted with rf filters. In addition, wires leading to the sample are fitted with rf filters with cutoff frequency ~ 400 kHz.

III. RESULTS

First, we qualitatively demonstrate the extreme sensitivity of the vortex state to external electromagnetic radiation. Figures 2(a)–2(b) show the resistance versus magnetic field (R - H) curves measured at 300 mK and 2 K, respectively, with RC filters of different cutoff frequencies. The magnetic field, H , is applied perpendicular to the film plane ($\theta = 0$). These measurements are performed with a dc current, $I^{dc} = 80$ μ A,

which is much smaller than the flux flow critical current, $I_c \sim 0.3 - 1$ mA [Figs. 2(c) and 2(d)]. We checked that the resistance values remain unchanged when we used lower values of I^{dc} (see Appendix B). In this paper all resistance measurements are done with dc current of this value. The purple curve corresponds to the R - H measured without any external filter. A finite resistance appears above 8 kOe. With increasing field the resistance increases, passes through a shallow minimum, and then increases again above 70 kOe. Comparing with real-space STS imaging, it was shown in Ref. [13] that these fields correspond to the transition from a VS to HVF state and a HVF to IVL, respectively. The shallow minima in R and corresponding maxima in I_c are signatures of “peak effect” [16], which has been extensively studied and reported elsewhere [17]. However, as we perform the measurement with different RC filters, the resistance above 8 kOe gets progressively suppressed as we use filters with lower f_c . For the lowest cutoff frequency, $f_c \sim 340$ kHz, the resistance is below the sensitivity of our measurement up to 95 kOe. Thus, the resistive features associated with the structural transitions of the VL are only observed when the sample is exposed to external radio-frequency electromagnetic radiation. Similarly, the I - V characteristics of the sample measured with and without filter at 300 mK are shown in Appendix C.

To understand this effect more systematically we now investigate the response of the superconductor to a small controlled ac excitation. We first shield the sample using the RC filter with $f_c \sim 340$ kHz and then add a small ac current, I_f^{ac} (frequency $f < 340$ kHz), to the dc current ($I^{dc} = 80 \mu\text{A}$). Figures 3(a) and 3(b) show the variation of R (at 300 mK) as a function of the ac amplitude, $I_{100 \text{ kHz}}^{ac}$ ($f = 100$ kHz) in different magnetic fields. Up to 6 kOe, R remains zero within the sensitivity of our measurements even in the presence of ac excitation. However, above this field R strongly depends on the excitation and a small $I_{100 \text{ kHz}}^{ac}$ drives the sample from a zero-resistance state to a dissipative state. Above 60 kOe, a small resistance appears even with zero excitation current, but even there the ac excitation increases the resistance by orders of magnitude. Figures 3(c) and 3(d) show the variation of R as a function of f for a fixed amplitude, $I_f^{ac} = 6.7 \mu\text{A}$. Again a strong frequency response is observed above 6 kOe, where the resistance increases rapidly above 10 kHz. The peak in the frequency response around 55 kHz is an artifact caused by the broad frequency response of single-pole RC filter which slightly decreases the amplitude I_f^{ac} at higher frequencies. Figure 3(e) shows the R - H curves measured in the presence of different amplitudes of $I_{100 \text{ kHz}}^{ac}$. Comparing with Fig. 2(a), one can see that increasing $I_{100 \text{ kHz}}^{ac}$ has the same qualitative effect as exposing the sample to external electromagnetic radiation. Measurements performed at 2 K (not shown here) are very similar to those performed at 300 mK. The main change with temperature is that the threshold magnetic field above which we observe the sensitivity of the superconductor to an ac current comes down to a lower value with increase in temperature.

In the presence of magnetic field the transport properties of the superconductor are expected to be dominated by vortex dynamics. To investigate this further, the magnetoresistive response of the sample was measured by changing the

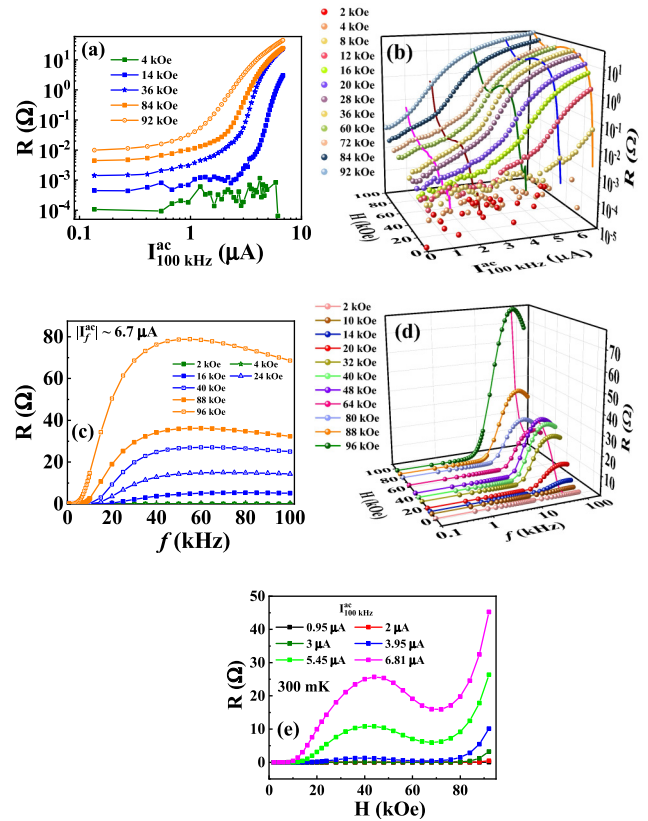


FIG. 3. (a), (b) dc resistance, R , as a function of the amplitude of ac current, $I_{100 \text{ kHz}}^{ac}$, in different magnetic fields at 300 mK. The lines in the three-dimensional plot (b) correspond to the variation of resistance for fixed $I_{100 \text{ kHz}}^{ac}$ as a function of magnetic field. (c), (d) dc resistance as a function of the frequency, f , of ac current with a fixed amplitude of $6.7 \mu\text{A}$, in different magnetic fields at 300 mK. The line in the three-dimensional plot (d) corresponds to the variation of resistance for $f = 50$ kHz as a function of magnetic field. (e) R - H at 300 mK measured in the presence of $I_{100 \text{ kHz}}^{ac}$ of different magnitudes. Measurements are done with RC filter with $f_c = 340$ kHz.

orientation of the sample with respect to the magnetic field. In Fig. 4(a) we compare the R - H in presence of $I_{100 \text{ kHz}}^{ac} = 2.3 \mu\text{A}$ for three orientations of the sample: (i) H perpendicular to the film plane (FP) (and current); (ii) H parallel to the FP and the current; and (iii) H parallel to the FP but perpendicular to the current. Since the thickness of our film is larger than twice the coherence length of a -MoGe, $\xi \sim 5$ nm [13], vortices can nucleate even when the magnetic field is in the plane of the film. In configuration (ii) the Lorentz force on the vortices due to the current is zero. Here the resistance remains below our sensitivity up to 100 kOe confirming that the observed resistance is caused by the flow of vortices. In configuration (iii) the Lorentz force per unit length, $\vec{J} \times \hat{n}\Phi_0$ (where \hat{n} is the unit vector along H and $\Phi_0 = h/2e$ is the flux quantum), on the vortices is the same as (i), but vortices are along the plane of the film. Here finite resistance appears only above 60 kOe. The insensitivity of the superconductor to the ac excitation until much larger fields than configuration (i) reflects the fact that the long vortex lines in this configuration are more strongly pinned than in

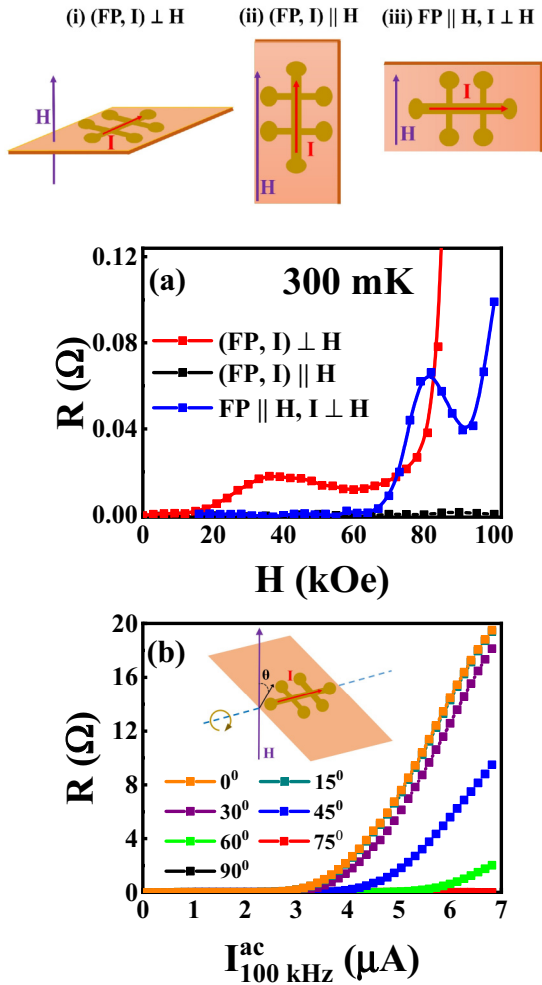


FIG. 4. (a) dc resistance, R , versus magnetic field at 300 mK with $I_{100 \text{ kHz}}^{\text{ac}} = 2.3 \mu\text{A}$, in three different sample orientations with respect to the magnetic field as shown above the panel. (b) dc resistance as a function of the ac current amplitude at 30 kOe, $I_{100 \text{ kHz}}^{\text{ac}}$, with magnetic field, H , at different angles, θ , with respect to the normal to the film plane, while the current is kept perpendicular to the H . (Inset) Schematic of the field orientation with respect to magnetic field and current; the black arrow denotes the normal to the film plane. Measurements are done with RC filter with $f_c = 340 \text{ kHz}$.

the case where the magnetic field is perpendicular to the film plane. In addition, between 60 and 100 kOe the resistance shows a pronounced nonmonotonic behavior reminiscent of the peak effect. However, since the sample is expected to have between 1 and 2 vortices on its width, this behavior is difficult to understand based on conventional explanations of peak effect [16] which involve a vortex lattice, and needs to be investigated in the future. In Fig. 4(b) we plot the resistance as a function of $I_{100 \text{ kHz}}^{\text{ac}}$ at 30 kOe for different angles (θ) of H with the normal to the FP, but keeping the current perpendicular to H . The length of the vortex is given by $t/\cos(\theta)$, where t is the film thickness. The sensitivity of the resistance to $I_{100 \text{ kHz}}^{\text{ac}}$ gradually decreases with increasing θ and goes below the sensitivity of our measurements for $\theta \geq 75^\circ$. These results confirm that the observed sensitivity of the superconductor is fundamentally linked to the vortex

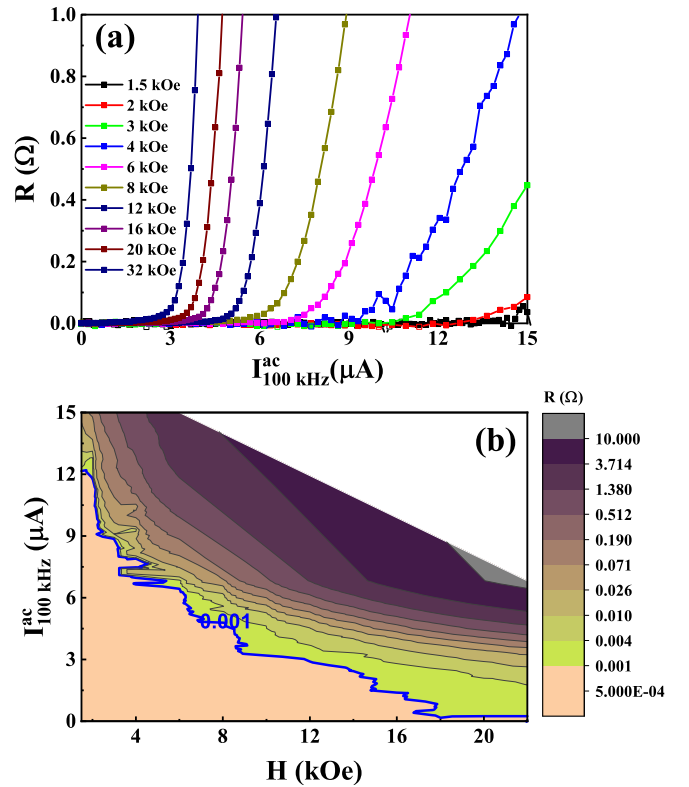


FIG. 5. (a) dc resistance, R , as a function of $I_{100 \text{ kHz}}^{\text{ac}}$ in different magnetic fields at 300 mK. (b) Intensity plot of R as a function of $I_{100 \text{ kHz}}^{\text{ac}}$ and magnetic field, H . The blue line shows the contour for which $R \approx 1 \text{ m}\Omega$. Measurements are done with RC filter with $f_c = 340 \text{ kHz}$.

state, and the vortices in different configurations can respond differently to radio-frequency ac perturbation.

Finally, we would like to note that while at low fields the zero-resistance state observed with H perpendicular to FP is robust to small ac excitations, it is nevertheless possible to destroy that by increasing the amplitude of ac current. This is shown in Fig. 5(a) where $I_{100 \text{ kHz}}^{\text{ac}}$ is increased up to a much larger value. This raises the obvious question on whether the identification of the VL at low fields and at intermediate fields as distinct state, namely VS and HVF, is meaningful. This question is particularly important since at low fields it is difficult to quantitatively determine the metrics of positional and orientational order within the limited field of view of STS that would allow us to discriminate between a VS and HVF from structural parameters of the VL alone. To address this, in Fig. 5(b) we plot R at 300 mK in the form of an intensity plot as a function of $I_{100 \text{ kHz}}^{\text{ac}}$ and H . (A measurable heating on the temperature sensor placed next to the sample is only observed for $I_{100 \text{ kHz}}^{\text{ac}} > 14 \mu\text{A}$.) The deep-blue line shows contour where R exceeds 1 mΩ, the sensitivity of our measurement. We observe that threshold in $I_{100 \text{ kHz}}^{\text{ac}}$ where a measurable resistance appears rapidly decreases with magnetic field and drops below our resolution of $0.3 \mu\text{A}$ above 17 kOe. This indicates the collapse of a pinning-related energy scale which renders the vortex lattice susceptible to very small perturbations. We believe that it is this energy scale that demarcates the low-field state, identified

earlier as a VS with the HVF at intermediate fields. However, this needs to be confirmed through more in-depth theoretical analysis.

IV. DISCUSSION

The most important question that arises from these measurements is why the transport properties of *a*-MoGe film display this extreme sensitivity to very small radio-frequency perturbations, whereas bulk superconductors remain largely unaffected. In our experiments we observe that the presence of very weakly pinned two-dimensional vortices plays a central role in the observed behavior. Since at finite frequencies vortices can dissipate energy to the electrons even with a subcritical drive current, in principle it is possible for the sample to get overheated. A simplistic estimate of the extent of overheating required to produce an effect of the magnitude observed in our experiments can be obtained by comparing the resistance versus temperature (R - T) of the film measured, for example, at 40 kOe without filter and with an RC filter with $f_c = 340$ kHz [Fig. 6(a)]. Comparing the temperature at which the R - T curve with filter reaches the same resistance as that of the R - T curve without filter at 300 mK, it would require the sample to get overheated by about 4 K to observe this effect. An equilibrium heating of the sample by such large amount is impossible without manifesting as a corresponding increase in the temperature measured on the temperature sensor placed next to the sample which we do not see. On the other hand, in Ref. [14] it was suggested that the electrons could get overheated with respect to the phonons by several kelvin due to weak electron-phonon coupling at low temperatures. Such a nonequilibrium overheating would not reflect on the temperature sensor which is electrically isolated from the sample. However, it will alter other superconducting properties that depend on the electronic temperature, such as the flux-flow resistance, R_{ff} , for $I > I_c$. To verify this, in Fig. 6(b) we plot the I - V characteristics in a field of 40 kOe (300 mK) with and without filter. The linear slope of the I - V curve in the flux-flow regime ($I > I_c$) gives R_{ff} which is identical for the two curves even though the I - V characteristics at low bias [inset of Fig. 6(b)] are significantly different. From the Bardeen-Stephen model [18,19], R_{ff} is given by $R_{ff} = R_N(\frac{H}{H_{c2}(T)})$, where R_N is the normal state resistance and H_{c2} is the upper critical field. Since H_{c2} decreases with increase in temperature one would have expected a significant increase in R_{ff} if the electrons were overheated. Similarly, the inset of Fig. 2(b) shows that the R - H curves measured with or without filter merge at high fields, implying that H_{c2} does not change significantly between the two. These observations are clearly incompatible with a large overheating of the electronic bath.

In this context, it is interesting to note that the influence of low-frequency magnetic excitation on the pinning properties of weakly pinned superconducting single crystals has been identified almost two decades ago [20], and has subsequently been used to unveil thermodynamic phases of the underlying vortex lattice [21,22]. The basic principle behind these experiments is as follows. In the presence of pinning the vortices can get trapped into metastable configurations; the application of a shaking field allows the vortices to overcome

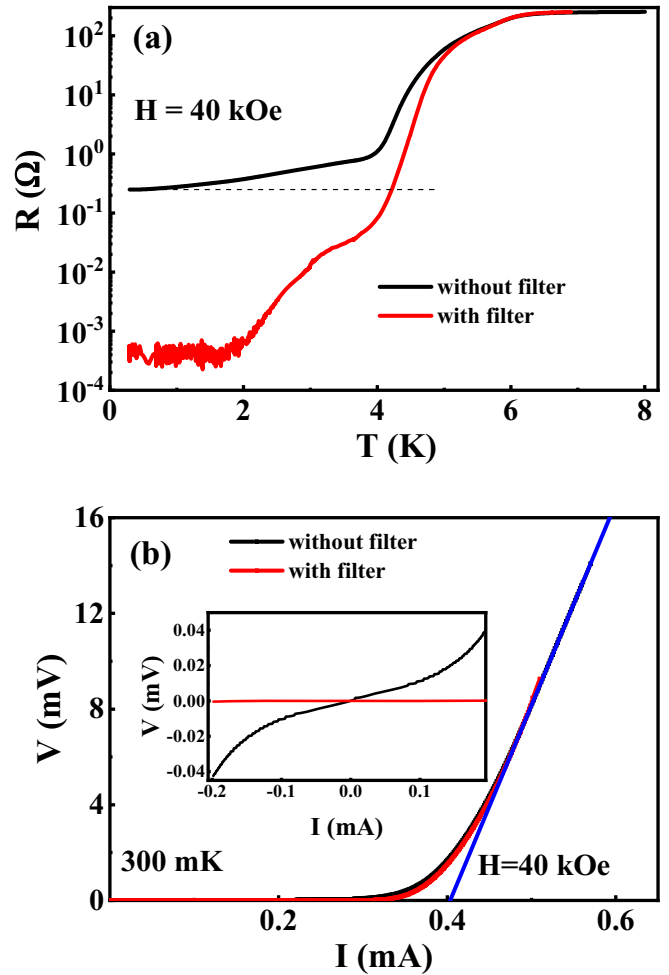


FIG. 6. (a) dc resistance, R , as a function of temperature, T measured at 40 kOe, without RC filter and with RC filter with $f_c = 340$ kHz. The dotted line denotes the resistance measured at 300 mK when the measurement is done without a filter. (b) I - V characteristics of the sample at 40 kOe, 300 mK without and with the same filter; (Inset) expanded view of the graph at low currents.

the pinning barrier and relax into their true equilibrium configuration. Recently this has been also confirmed from structural measurements of the VL using [23,24] STS and neutron diffraction [25]. The effect that we observe here is also related to pinning, but distinct from the ones mentioned above. Since the pinning in the *a*-MoGe film is extremely weak we cannot discern the existence of any metastable states in zero-field-cooled and field-cooled measurements of ac susceptibility or in real-space imaging [26]. Thus it appears that here the VL can always find its equilibrium configuration. Here the effect of radio-frequency radiation seems to be a dynamic phenomenon, whereby the mobility of vortices in the HVF state increases by orders of magnitude when the vortices are shaken, producing a measurable linear dc resistance well below I_c . This could happen in several possible ways. For example, shaking the vortices could generate additional topological defects rendering the vortices more mobile. Alternatively, shaking the vortices could also lead to modifications in the collective activation barrier for thermally activated flux flow.

However, a thorough theoretical analysis is needed in order to identify the precise microscopic mechanism and conduct further quantitative analysis.

Finally, it is interesting to try to identify the source of electromagnetic radiation that could give rise to the observed effect when measurements are performed without filter. We observe that using a low-pass filter with 340 kHz cutoff effectively removes the effect of ambient radiation, even though the sample responds to much lower frequencies. To understand this, we first note that most wireless communicating devices, such as Wi-Fi, Bluetooth, wireless mouse, and keyboard work at frequency ranges well above 100 MHz. FM radio stations which are another source of electromagnetic radiations transmit at carrier frequencies of tens of MHz. All these are easily filtered out with filters with much higher cutoff. However, in the city of Mumbai we found six short- and medium-wave AM radio stations transmitting in hundreds of kHz to few MHz frequency range [27]. The lowest-frequency ambient radiation source that we could identify is Mumbai B (Asmita Vahini) radio channel transmitting at 558 kHz. Once the filter cutoff is set to lower than this value, the spectrum is more or less silent and any remaining radiation is not strong enough to drive the resistance above our limit of detection.

V. CONCLUSION

In conclusion, we have shown that the two-dimensional vortex states in weakly pinned *a*-MoGe thin film are extremely susceptible to external electromagnetic excitations. The most intriguing part of this study is the very low frequency and amplitude threshold of ac excitation above which we see this effect. We believe that this is due to the formation of vortex fluid states with very low mobility of the vortices. Thus even though the vortex motions at low currents in these fluid states do not produce any detectable resistance, the mobility of the vortices gets vastly enhanced in the presence of an external electromagnetic excitations. It would be interesting to explore to what extent this could be generic for other systems, such as InO_x and few-layered NbSe_2 which display similar sensitivity in the presence of magnetic field.

ACKNOWLEDGMENTS

We would like to thank Vadim Geskenbein for drawing our attention to the possible discrepancy between STS and transport data. We would also like to thank Benjamin Sa-cepe, I. Tamir, Dan Shahar, and Peter Armitage for valuable discussions. Finally, we would like to thank the organizers of the workshop ‘‘The challenge of 2-dimensional superconductivity’’ at Lorentz Center, The Netherlands for a vibrant discussion on the effect of high-frequency electromagnetic noise on the transport properties of two-dimensional superconductors. This work was financially supported by Department of Atomic Energy, Government of India (Grant No. 12-R&D-TFR-5.10-0100).

S.D. performed the transport measurements and analyzed the data. I.R. performed the STS measurements and analyzed the data. J.J. and V.B. prepared the *a*-MoGe film and performed basic characterization. S.M. carried out complementary magnetic measurements and wrote the instrument interface codes for transport measurements. P.R. conceptualized the problem, supervised the project, and wrote the paper with input from all authors.

APPENDIX A: DIFFUSION CONSTANT OF THE VORTICES FROM REAL-SPACE STS IMAGES

The vortex diffusion constant, D , which is related to the resistance observed in the mixed state of a type II superconductor, can in principle be obtained by tracking the motion of vortices as a function of time as was done in Ref. [13]. From microscopic random-walk viewpoint of the Brownian motion, the mean-square displacement ($\langle r^2 \rangle$) is related to the diffusion coefficient (D) as, $\langle r^2 \rangle = 4Dt$, where t is time [28]. To experimentally determine $\langle r^2 \rangle$ we capture 12 successive images of the VL using STS staying at the same field, at intervals of 15 min. The trajectory of each vortex as a function of time is obtained by comparing each successive image. An example, at 55 kOe, 450 mK is shown in Fig. 7.

In Fig. 8 we plot the mean-square displacement normalized to the vortex lattice constant, a , as a function of time at different fields. At fields higher than 70 kOe, the variation

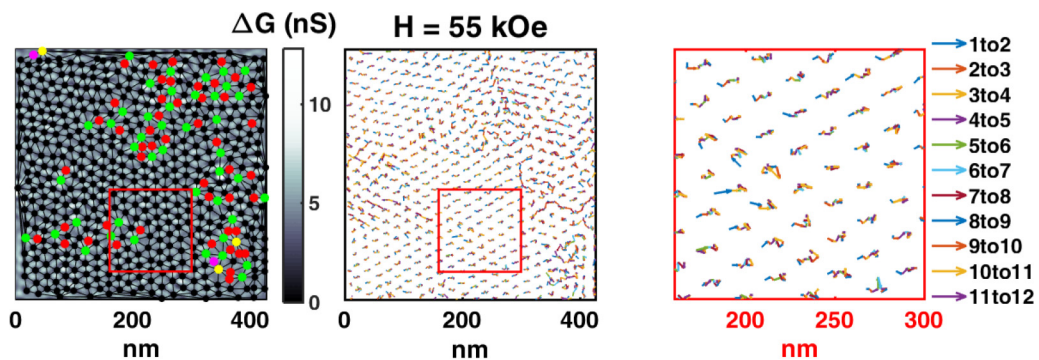


FIG. 7. (Left panel) First image of 12 consecutive vortex images at 450 mK for 55 kOe. VL is Delaunay triangulated to find topological defects (denoted as red, green, magenta, and yellow dots) corresponding to five-, seven-, four-, and eightfold coordination. (middle panel) Arrow map of the vortex motion, in which each arrow gives displacement for every vortex through individual steps of 12 consecutive images. (right panel) Enlarged view of the red box in the middle panel.

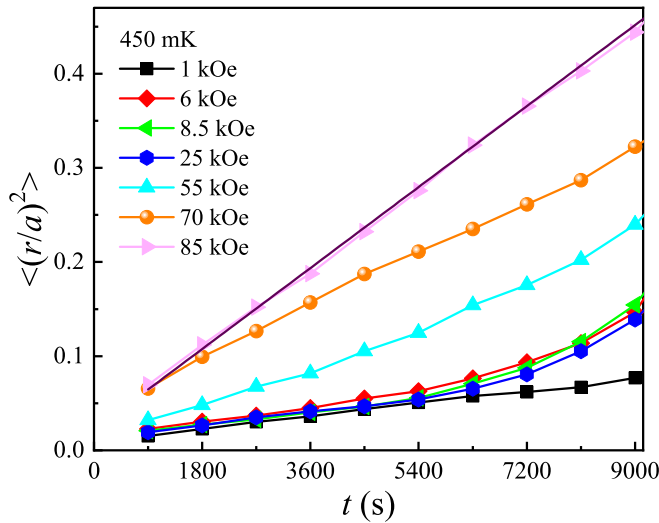


FIG. 8. The mean-square displacements in units of lattice constant, a , as a function of time determined from the 12 images at different magnetic fields at 450 mK. The magenta straight line is a linear fit to the 85 kOe data.

is linear as expected for Brownian motion in an isotropic vortex liquid. To obtain an upper bound to the diffusion constant, we calculate the diffusion constant at 85 kOe as, $D = 3.23632 \times 10^{-21} \text{ m}^2/\text{s}$.

We can now calculate the resistivity that would arise from the vortex motion. Assuming that the motion is thermal in origin, the mobility of the vortices is $\mu = D/k_B T$ (where k_B is the Boltzmann constant). This gives the effective viscosity of the vortices as $\eta = \frac{1}{\mu d} = \frac{k_B T}{D d} = 1.37063 \times 10^5 \text{ kg m}^{-1} \text{ s}^{-1}$. This would give a thermally activated flux-flow resistivity [19], $\rho_{TAF} = B \times \frac{\Phi_0}{\eta} = 1.28371 \times 10^{-19} \text{ } \Omega \text{ m}$, which is well below the sensitivity of our measurements. Though this kind of analysis is not completely free from our inability to determine large flux jumps given the indistinguishability of the vortices, this gives an order of magnitude estimation of the resistivity which one would expect in the vortex fluid phases. Thus given the current scenario in absence of external electromagnetic perturbation, one would expect no appearance of resistivity in the HVF phase.

APPENDIX B: RESISTANCE MEASUREMENT WITH DIFFERENT dc CURRENTS

To understand the effect of I_f^{ac} on the resistance it is important to ensure that I^{dc} is kept low enough such that nonlinear resistive effects do not result from the dc current drive itself. In Fig. 9(a) we show R - H measured without filter for $I^{dc} = 10, 20, 50,$ and $80 \text{ } \mu\text{A}$. For $H < 90 \text{ kOe}$, which is the range of field of interest in this work, the resistance is identical for all four curves within the accuracy of the measurement. This can also be seen from the linearity of the I - V curves shown in the inset. (For $H > 90 \text{ kOe}$ there is an increase in R for larger I^{dc} since I_c comes down rapidly.) In Fig. 9(b) we show the variation of R as a function of $I_{100\text{kHz}}^{ac}$ at 25 kOe, 300 mK using different values of I^{dc} . Except for the increase in noise at lower currents again the curves for different I^{dc} are

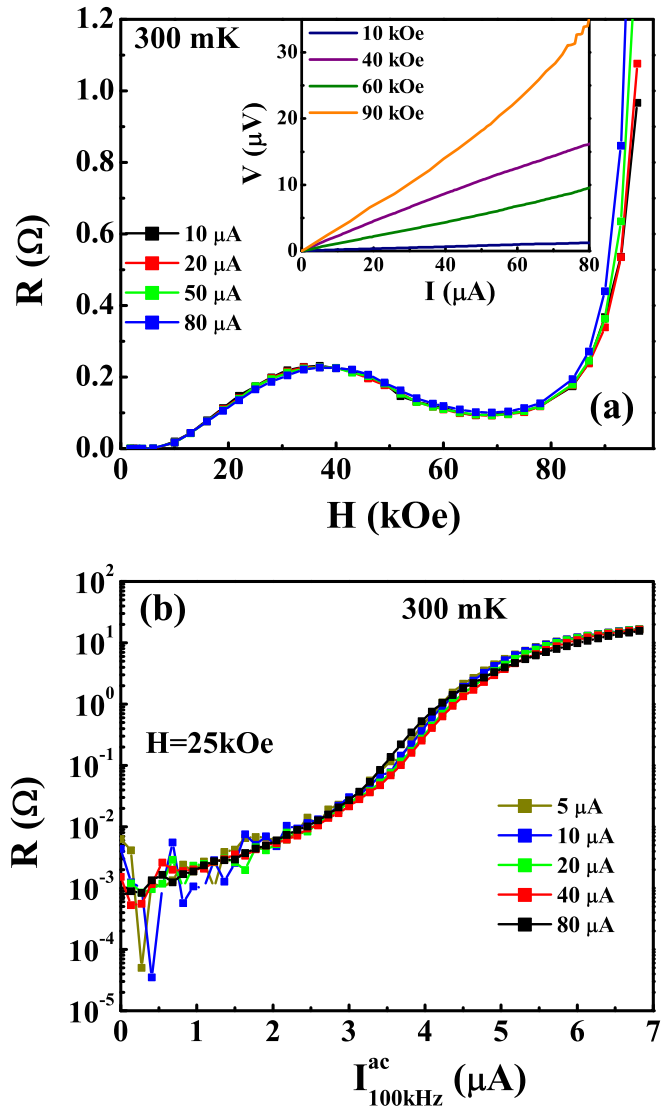


FIG. 9. (a) Resistance, R , as a function of magnetic field 300 mK, for $I^{dc} = 10, 20, 50,$ and $80 \text{ } \mu\text{A}$. The data are taken without filter. (Inset) I - V characteristics (low current regime, $I \ll I_c$) at 300 mK. (b) R as a function of $I_{100\text{kHz}}^{ac}$ for $I^{dc} = 5, 10, 20, 40,$ and $80 \text{ } \mu\text{A}$ at 25 kOe, 300 mK; in this measurement RC filter with $f_c = 340 \text{ kHz}$ was used.

similar. All other measurements in the paper are done with $I^{dc} = 80 \text{ } \mu\text{A}$.

APPENDIX C: I - V CHARACTERISTICS WITH AND WITHOUT FILTER

In Figs. 10(a)–10(e) we show the I - V characteristics at 300 mK in five different magnetic fields, measured without filter and with an RC filter with $f_c = 340 \text{ kHz}$ plotted in log-log scale. As shown in Fig 6(b) in the flux-flow regime above I_c , the two curves merge with each other. However, the behavior is very different in the thermally activated flux flow regime, $I \ll I_c$. Here, the voltage is orders of magnitude larger when measured without filter. Since the I - V characteristics in the flux-flow regime is not significantly affected by radio-frequency excitation, the values of I_c extracted from

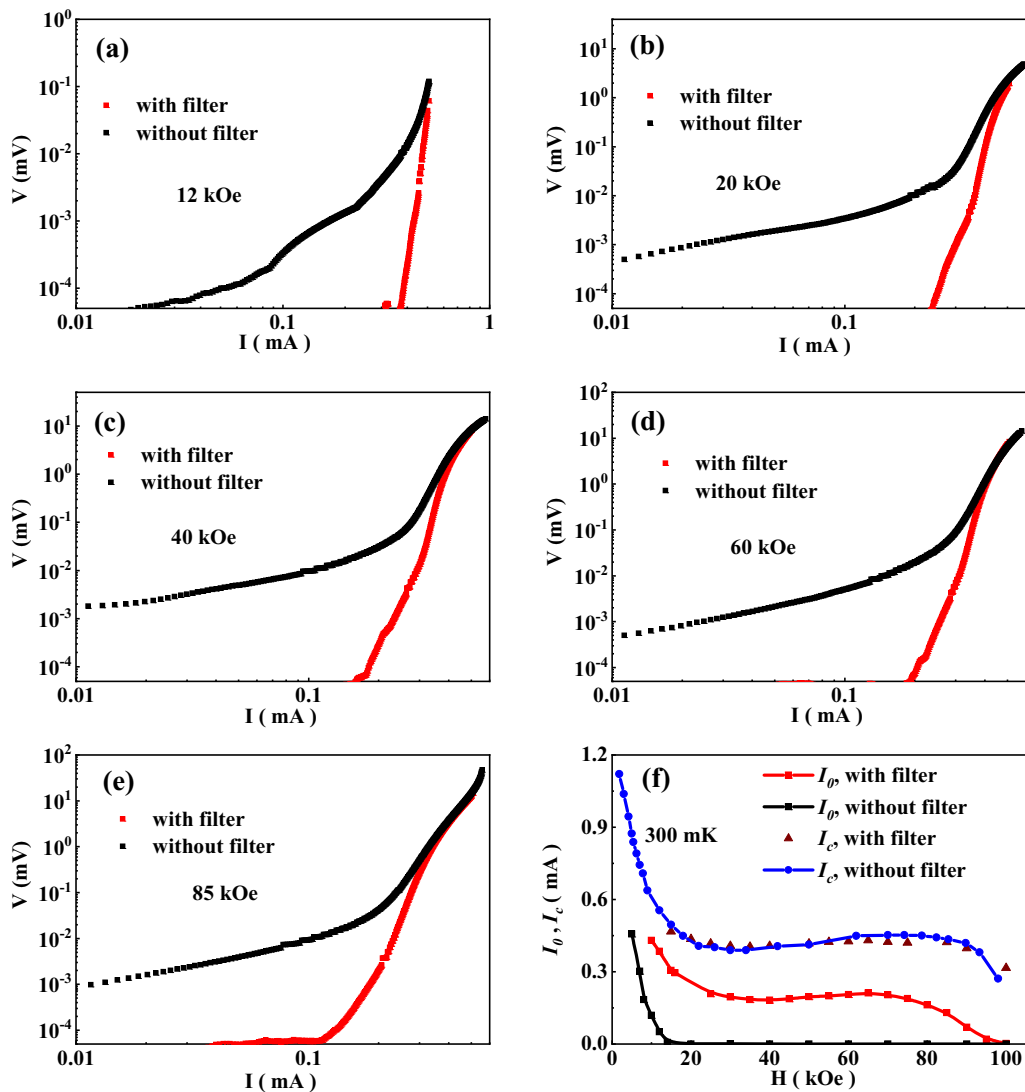


FIG. 10. (a)–(e) I - V characteristics measured without and with RC filter ($f_c = 340$ kHz) plotted in log-log scale at 300 mK for five different magnetic fields. (f) Variation of I_0 and I_c extracted from the I - V curves obtained without and with filter.

the two sets of measurements [Fig. 10(f)] are also close to each other. However, we can also define a notional depinning current, I_0 , at which a measurable voltage appears. Taking this threshold voltage as 100 nV we plot in the same graph

I_0 extracted from the two sets of measurements, whereas with filter, I_0 , has the same qualitative variation as I_c , when measured without filter it decreases rapidly to zero above 17.5 kOe.

[1] A. A. Abrikosov, The magnetic properties of superconducting alloys, *J. Phys. Chem. Solids*, **2**, 199 (1957).
 [2] L. P. Lévy, Vortices in Type II Superconductors, in *Magnetism and Superconductivity: Texts and Monographs in Physics* (Springer, Berlin, 2000).
 [3] S. Sengupta, C. Dasgupta, H. R. Krishnamurthy, G. I. Menon, and T. V. Ramakrishnan, Freezing of the Vortex Liquid in High- T_c Superconductors: A Density-Functional Approach, *Phys. Rev. Lett.* **67**, 3444 (1991).
 [4] A. De Col, G. I. Menon, and G. Blatter, Density functional theory of vortex lattice melting in layered superconductors: A mean-field substrate approach, *Phys. Rev. B* **75**, 014518 (2007).

[5] E. M. Forgan, S. J. Levett, P. G. Kealey, R. Cubitt, C. D. Dewhurst, and D. Fort, Intrinsic Behavior of Flux Lines in Pure Niobium near the Upper Critical Field, *Phys. Rev. Lett.* **88**, 167003 (2002).
 [6] C. J. Bowell, R. J. Lycett, M. Laver, C. D. Dewhurst, R. Cubitt, and E. M. Forgan, Absence of vortex lattice melting in a high-purity Nb superconductor, *Phys. Rev. B* **82**, 144508 (2010).
 [7] A. Yazdani, C. M. Howald, W. R. White, M. R. Beasley, and A. Kapitulnik, Competition between pinning and melting in the two-dimensional vortex lattice, *Phys. Rev. B* **50**, R16117 (1994).

- [8] P. Berghuis, A. L. F. van der Slot, and P. H. Kes, Dislocation-Mediated Vortex-Lattice Melting in Thin Films of a-Nb₃Ge, *Phys. Rev. Lett.* **65**, 2583 (1990).
- [9] S. Uji, Y. Fujii, S. Sugiura, T. Terashima, T. Isono, and J. Yamada, Quantum vortex melting and phase diagram in the layered organic superconductor κ -(BEDT-TTF)₂Cu(NCS)₂, *Phys. Rev. B* **97**, 024505 (2018).
- [10] H. Pastoriza, M. F. Goffman, A. Arribére, and F. de la Cruz, First Order Phase Transition at the Irreversibility Line of Bi₂Sr₂CaCu₂O₈, *Phys. Rev. Lett.* **72**, 2951 (1994).
- [11] E. Zeldov, D. Majer, M. Konczykowski, V. B. Geshkenbein, V. M. Vinokur, and H. Shtrikman, Thermodynamic observation of first-order vortex-lattice melting transition in Bi₂Sr₂CaCu₂O₈, *Nature (London)* **375**, 373 (1995).
- [12] A. Schilling, R. A. Fisher, N. E. Phillips, U. Welp, D. Dasgupta, W. K. Kwok, and G. W. Crabtree, Calorimetric measurement of the latent heat of vortex-lattice melting in untwinned YBa₂Cu₃O_{7- δ} , *Nature (London)* **382**, 791 (1996).
- [13] I. Roy, S. Dutta, A. N. Roy Choudhury, S. Basistha, I. Maccari, S. Mandal, J. Jesudasan, V. Bagwe, C. Castellani, L. Benfatto, and P. Raychaudhuri, Melting of the Vortex Lattice through Intermediate Hexatic Fluid in an a-MoGe Thin Film, *Phys. Rev. Lett.* **122**, 047001 (2019).
- [14] I. Tamir, A. Benyamini, E. J. Telford, F. Gorniaczyk, A. Doron, T. Levinson, D. Wang, F. Gay, B. Sacépé, J. Hone, K. Watanabe, T. Taniguchi, C. R. Dean, A. N. Pasupathy, and D. Shahar, Sensitivity of the superconducting state in thin films, *Sci. Adv.* **5**, eaau3826 (2019).
- [15] A. Kamlapure, G. Saraswat, S. C. Ganguli, V. Bagwe, P. Raychaudhuri, and S. P. Pai, A 350 mK, 9 T scanning tunnelling microscope for the study of superconducting thin films on insulating substrates and single crystals, *Rev. Sci. Instrum.* **84**, 123905 (2013).
- [16] M. J. Higgins and S. Bhattacharya, Varieties of dynamics in a disordered flux-line lattice, *Physica C* **257**, 232 (1996).
- [17] S. Dutta, I. Roy, S. Basistha, S. Mandal, J. Jesudasan, V. Bagwe, and P. Raychaudhuri, Collective flux pinning in hexatic vortex fluid in a-MoGe thin film, *J. Phys.: Condens. Matter* **32**, 075601 (2020).
- [18] J. Bardeen and M. J. Stephen, Theory of the motion of vortices in superconductors, *Phys. Rev.* **140**, A1197 (1965).
- [19] M. Tinkham, *Introduction to Superconductivity* (McGraw-Hill, New York, 1996).
- [20] M. Willemin, C. Rossel, J. Hofer, H. Keller, A. Erb, and E. Walker, Strong shift of the irreversibility line in high- T_c superconductors upon vortex shaking with an oscillating magnetic field, *Phys. Rev. B* **58**, R5940 (1998).
- [21] N. Avraham, B. Khaykovich, Y. Myasoedov, M. Rappaport, H. Shtrikman, D. E. Feldman, T. Tamegai, P. H. Kes, M. Li, M. Konczykowski, K. van der Beek, and E. Zeldov, Inverse melting of the vortex lattice, *Nature (London)* **411**, 451 (2001).
- [22] N. Avraham, B. Khaykovich, Y. Myasoedov, M. Rappaport, H. Shtrikman, D. E. Feldman, E. Zeldov, T. Tamegai, P. H. Kes, M. Li, M. Konczykowski, and K. van der Beek, First-order disorder-driven transition and inverse melting of the vortex lattice, *Phys. C: Supercond.* **369**, 36 (2002).
- [23] S. C. Ganguli, H. Singh, G. Saraswat, R. Ganguly, V. Bagwe, P. Shirage, A. Thamizhavel, and P. Raychaudhuri, Disordering of the vortex lattice through successive destruction of positional and orientational order in a weakly pinned Co_{0.0075}NbSe₂ single crystal, *Sci. Rep.* **5**, 10613 (2015).
- [24] S. C. Ganguli, H. Singh, I. Roy, V. Bagwe, D. Bala, A. Thamizhavel, and P. Raychaudhuri, Disorder-induced two-step melting of vortex matter in Co-intercalated NbSe₂ single crystals, *Phys. Rev. B* **93**, 144503 (2016).
- [25] M. Marziali Bermudez, M. R. Eskildsen, M. Bartkowiak, G. Nagy, V. Bekeris, and G. Pasquini, Dynamic Reorganization of Vortex Matter into Partially Disordered Lattices, *Phys. Rev. Lett.* **115**, 067001 (2015).
- [26] For example, the field-cooled and zero-field-cooled susceptibility measurements fall exactly on the top of one another even for fields as low as 500 Oe; see supplementary material in Ref. [13].
- [27] For a list of radio stations in Mumbai, see <http://worldradiomap.com/in/mumbai>.
- [28] K. A. Dill and S. Bromberg, Molecular driving forces: Statistical thermodynamics in biology, chemistry, physics, and nanoscience, *Briefings Bioinf* **4**, 382 (2003).